Stockholm University

Bachelor Thesis

Degree Project in Marine Geology 15 hp

Sea level rise and grain size changes in two sediment cores from the Herald Canyon, Western Arctic Ocean

Henrik Tarras

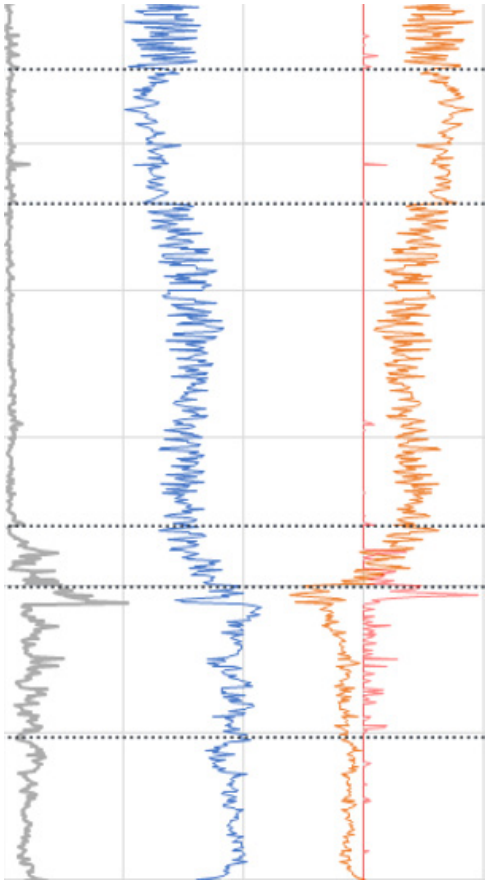

Stockholm 2017

Department of Geological Sciences
Stockholm University
SE-106 91 Stockholm
Sweden

Table of contents

Abstract.
Herald Canyon is located in the northwestern part of the Chukchi Sea. This study presents grain size distribution from two cores, SWERUS-L2-4-PC1 and SWERUS-L2-5-GC1, taken from Herald Canyon during Leg 2 of the SWERUS-C3 expedition in 2014, which show how the site has changed from near-shore to a continental shelf setting due to increasing sea level. The flooding of Bering Strait at 11,000 cal yr BP is correlated with abrupt shifts in grain size that, when integrated with an age model, show signs of both winnowing and erosion from paleocurrents. The erosional horizon, seen clearly in the grain size data, occurs after 11,000 cal yr BP, when the coring site would have been at a depth of over 70 meters. Therefore, it likely formed in response to the opening of Bering Strait and the inflow of Pacific waters to the Arctic during the early Holocene, rather than erosion related to shoreline transgression.

1 Introduction.

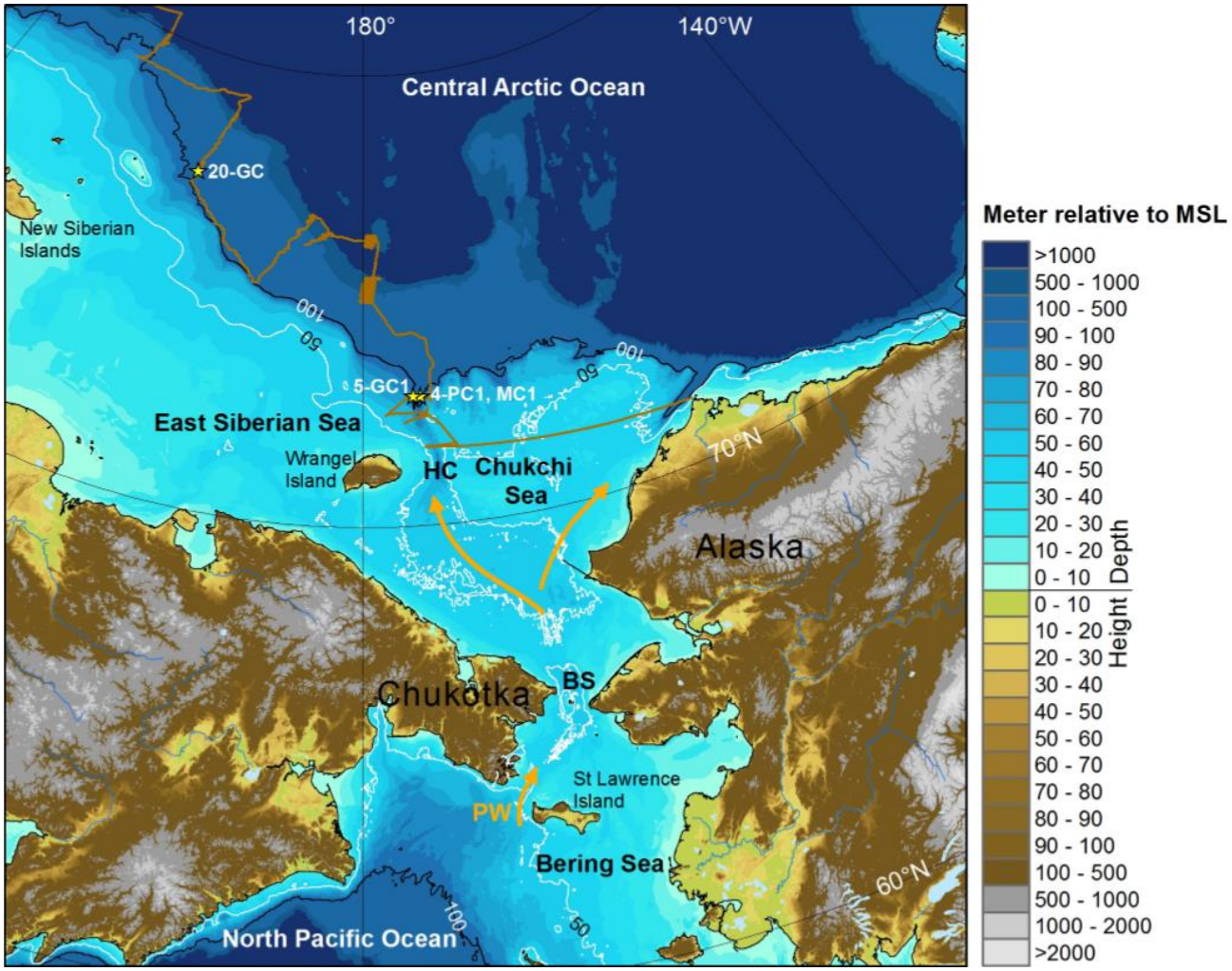

Figure 1: Map showing the Chukchi Sea area, with present day depths, from Cronin et al., 2017. The brown lines are the path that was taken during Leg 2 of the SWERUS-C3 expedition. Orange arrows illustrate modern pathways of Pacific water into the Arctic ocean.

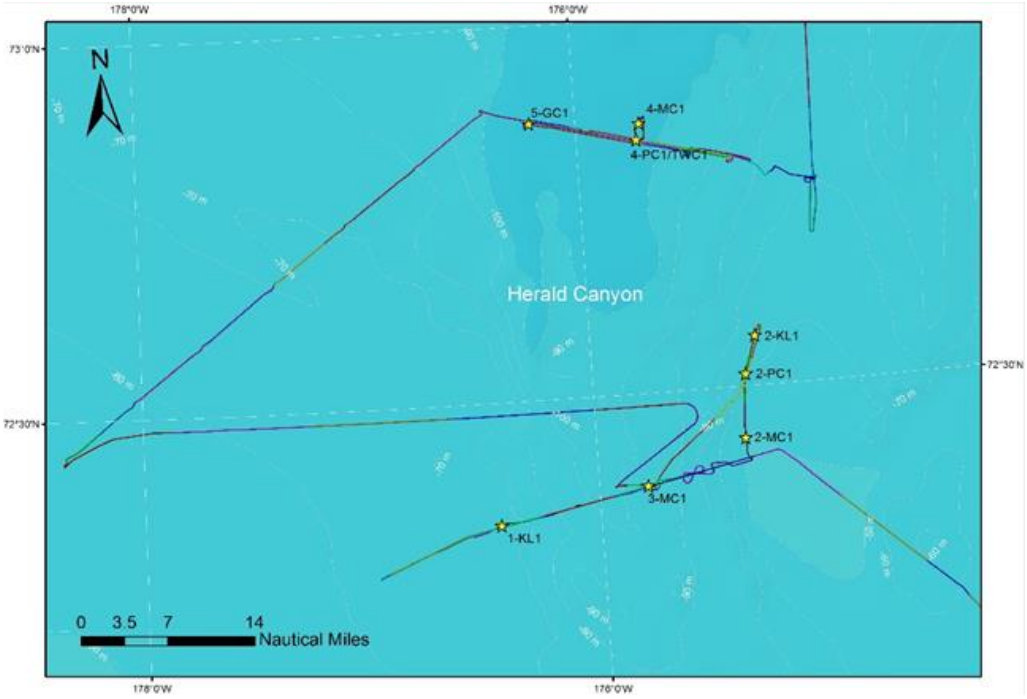

Figure 2: Close-up of sampling stations and ship track lines in Herald Canyon during the SWERUS-C3 expedition (from Jakobsson et al., 2017). Cores discussed in this study, 5-GC1 and 4-PC1, are located along transect 4.

Herald Canyon is situated in the western Arctic (Figure 1), on the Chukchi shelf, north of the shallow (~53 m) Bering Strait, running roughly along a north-south direction (Figure 2). Today, Pacific water enter in the Arctic through the Bering Strait (Woodgate et al., 2015), and reaches Herald Canyon. However, during the last glacial maximum, the sea level was 120 meters lower than present (Figure 3), and Bering Strait was subsequently above sea level. The flooding of Bering Strait after the last glacial maximum marks an important paleoenvironmental change. There is evidence for inflow of Pacific water into the Arctic after the opening, both in the past and the present (Jakobsson et al., 2017), and sea-ice ocean models show that a spatially extensive spreading of Pacific water can have an adverse effect on sea ice growth (Watanabe and Hasumi, 2009), which in turn may have affected paleoclimate.

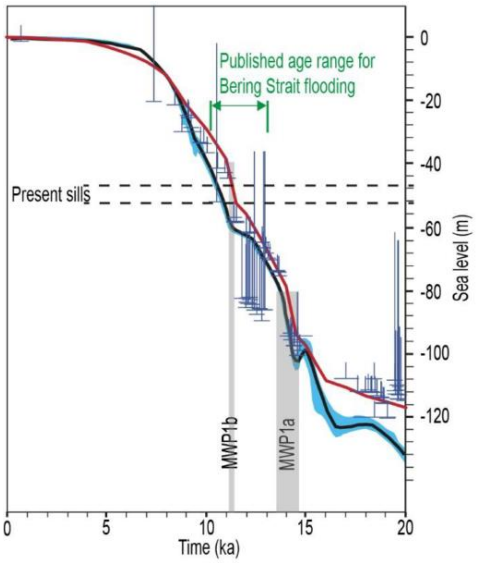

Figure 3: From Jakobsson et al., 2017, showing sea-level estimations during the last 20,000 years. Meltwater Pulse 1a (MWP1a) and Meltwater Pulse 1b (MWP1b) is seen as grey bars. The depth of the present sills in Bering Strait are the horizontal dotted lines. The red line is a model of sea-level history with ICE-5G(VM2) (Peltier and Fairbanks, 2006). The blue bars are predicted sea-level based on Barbados coral reef records. The black curve is the ice-volume equivalent sea-level change, and the vertical blue lines show its 95% probability limit, by Lambeck et al. (2014).

Recent work using seismic data and sediment cores collected on the SWERUS-C3 expedition to the Arctic has provided a new date of 11,000 cal yrs BP for the opening of the Bering strait upon deglaciation in the Holocene (Jakobsson et al., 2017). This comes from the analysis of two sediment cores, SWERUS-L2-4-PC1 and SWERUS-L2-2-PC1, recovered in Herald Canyon. The former contains a pronounced lithological change from nearshore to marine conditions, and is believed to contain a record of sea-level transgression during deglaciation, and the subsequent opening of the Bering Strait (Jakobsson et al., 2017).

Previous dates for the opening of Bering Strait were either maximum or minimum ages. Maximum age constraints were done by Elias et al. (1992) and Keigwin et al. (2006). Minimum age constraints have been based on the appearance of Bowhead whale remains in the Canadian Arctic (Dyke and Savelle, 2001) and the Pacific mollusk Cyrtodaria kurriana in the Canadian Arctic (England and Furze, 2008).

The age model for SWERUS-L2-4-PC1 was constructed by Jakobsson et al. (2017) using accelerator mass spectrometry (AMS) radiocarbon dating, at eight levels. Different ΔR values were used for calibrating pre-flood (50 ± 100) and post-flood dates (300 ± 200), since Pacific water has an impact on the reservoir (Jakobsson et al., 2017). For core 5-GC1 there is no age model, leading to limitations in comparison between the cores.

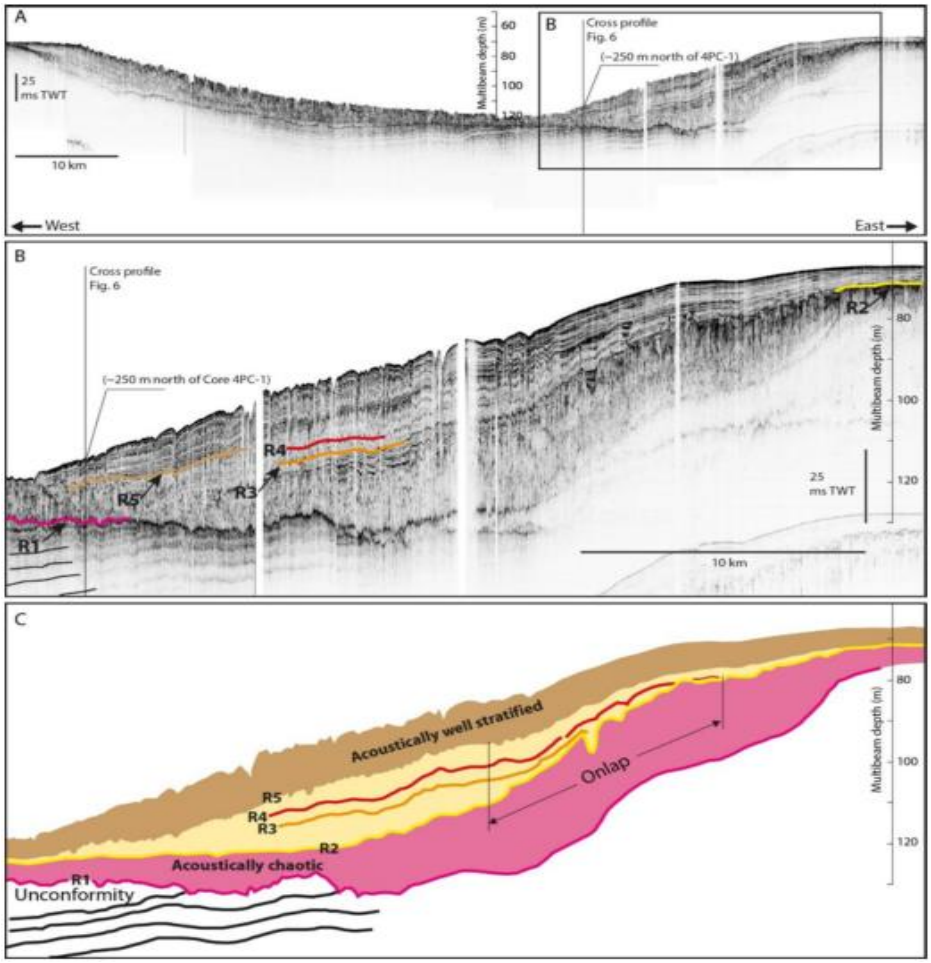

Figure 4: Chirp sonar sub-bottom profiles from Jakobsson et al., 2017. **A)** Transect 4 of Herald Canyon, the black bar is directly north of Core 4PC1. **B)** Close-up profile of the sub-bottom profile on the eastern part, where Core 4PC1 was retrieved. Reflectors R5 to R1 are marked. **C)** Interpretation of acoustic units, showing how the strata below reflector R2 is more acoustically varied.

From sub-bottom profiles, five reflectors have been identified (Jakobsson et al., 2017). R5, the shallowest one, marks a change between the overlying acoustically well-stratified sediments and a denser middle strata. Reflector R2 is situated between the middle strata and an acoustically chaotic one (Figure 4). Previous data have not allowed confirmation whether reflector R2 was penetrated. Reflectors R2, R3 and R4 exhibit onlap upslope, which is typical for transgression, and can hence be viewed as deposited after sea level started to rise. Reflector R5 can be linked to the transition from a near-shore to deep marine environment, as the lithological break is in proximity to it, which is further supported by the age model.

A clear break in the lithology of Core 4-PC1 is indicated by an apparently abrupt transition up-core from shallow, coastal conditions to fully marine conditions by 407 cm (Jakobsson et al., 2017; Cronin et al., 2017). Depending on how the age model is drawn, this can either be interpreted as an extensive hiatus, or a period of condensed sedimentation (Figure 5).

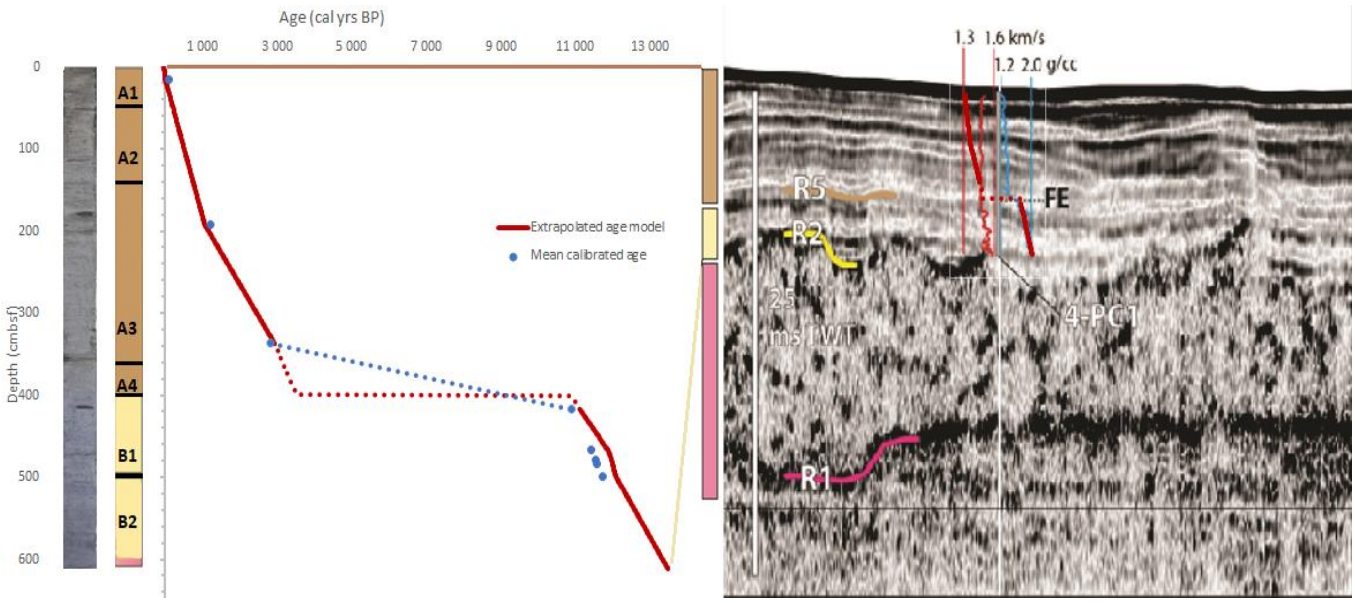

Figure 5: Core-seismic combination for SWERUS-L2-4-PC1 (modified from Figure 6 in Jakobsson et al., 2017) with variation in age as the red line and blue data points as mean calibrated ages. The dotted red line illustrates the interval of a possible hiatus. The blue dotted line shows a linear slope between measured depths that assumes condensed sedimentation instead of a hiatus. The lower pink portion of subunit B2 illustrates the possibility that the core penetrated reflector R2. Figures above the acoustic profile indicate bulk density, p-wave velocity and magnetic susceptibility.

The aim of this study is to investigate grain size variations in cores 4-PC1 and 5-GC1 to determine the possible nature of the lithologic transition from near-shore to open marine modes of sedimentation. The basic hypothesis is that a period of erosion during such a transition, will result in an abrupt coarsening of the grain size data, while a period of slow sedimentation would be dominated by fine grained material and lack abrupt changes in grain size.

2 Method.

2.1 Sediment Cores.

SWERUS-L2-4-PC1 was collected at a depth of 120 m at lat 72.838669, lon -175.7273 (Figure 2) on the eastern slope of Herald Canyon, and has a core length of 6.24 m. SWERUS-L2-5-GC1 was retrieved at 116 m water depth, lat 72.8696, lon -176.2077 (Figure 2), and is 1.42 m long (which includes the 0.36 m core catcher). It was taken from the western part of Herald Canyon, signified by less sedimentation, flatter slope

and a harder seafloor compared to the eastern part, based on interpretation of sub-bottom profiling (Jakobsson et al., 2017). Published age models were used for Core 4-PC1, but no dating has been done on 5-GC1.

2.2 Grain Size Measurements.

Grain size measurements were performed on the split core sections at 1 cm down-core resolution using a small spoon, and added to tubes containing 5 ml de-ionized water and 3 ml sodium-metaphosphate. The amount of sediment taken was not based on weight, but on apparent volume. The sediment was disaggregated by shaking, stirring and ultrasonication for 60 seconds or until no visible aggregates or floccules were present. The grain size was then analyzed with laser granulometry, using the MasterSizer3000 by Malvern, which employs a laser diffraction method. This works by means of optical sensors measuring scattering of light which passes through the sample, based on known incident angles. Larger grains have smaller angles of scattering, while the opposite holds true for smaller grains.

The prepared samples were added to a Hydro LV module, which is used for dispersing wet samples and sending it to the main MasterSizer3000 unit. Using a custom Standard Operation Procedure (S.O.P.) they were sonicated for 60 seconds before being measured.

Deposition in marine settings often contains floccules and aggregates, and grain size analysis after disaggregation in the lab does not necessarily give a true picture of the depositional regime, since the sediments were not necessarily deposited in a disaggregated state (McCave et al., 2006).

The volume of sediment is one of the factors influencing laser obscuration in the MasterSizer3000, which is a measure of the percentage of light that does not reach the sensor through the fluid. Upon initiation of the project, a laser obscuration of 5-8 % was recommended as it is routinely used in the lab, but the official Malvern recommendation, as stated in the manual for the MasterSizer3000, for laser granulometry using the wet dispersion Hydro LV module for fine-grained sediment is 10-20%. To investigate any differences between these obscuration ranges in measured grain size distributions, resampling aiming at a 10-20% obscuration was done for the first 27 cm of SWERUS-L2-4-PC1 section 1.

2.3 Grain size data processing.

The MasterSizer3000 presents results in bin sizes, which are the size classes that the grain size fractions are distributed over along a logarithmic scale, expressed as %volume of the sum of all measurements. The MasterSizer3000 was configured to make five measurements on each sample. These were then averaged, and calculations were based on the averages.

Mean grain size, standard deviation, skewness and kurtosis were calculated from the bin size values using the Geometric Method of Moments (Figure 6), (Blott and Pye, 2001), where m_m corresponds to the bin size (mid-point) and f is the %volume (or frequency) of the mid-point measurement. Standard deviation is a measure of how close the data is to the mean, which is systematically used in sedimentology as an expression of how well sorted the material is. Skewness is used for interpreting the symmetry of the data, where a higher (positive) value means that the the normal distribution curve has a tail extending more the right than to the left. This means that a high ratio of coarse-grained to fine-grained sediment will have a tail to the left of the normal distribution, and yield a negative skewness value. Kurtosis on the other hand indicates how the tails of the distribution are weighted compared to the normal distribution curve, where a higher value means thicker tails. Thus, a grain size distribution that mainly plots in one size class will have a high kurtosis, signified by a sharp distribution curve.

Mean	Standard deviation	Skewness	Kurtosis
$\bar{x}_g = \exp \frac{\Sigma f \ln m_m}{100}$	$\sigma_g = \exp \sqrt{\frac{\Sigma f (\ln m_m - \ln \bar{x}_g)^2}{100}}$	$Sk_g = \frac{\Sigma f (\ln m_m - \ln \bar{x}_g)^3}{100 \ln \sigma_g{}^3}$	$K_g = \frac{\Sigma f (\ln m_m - \ln \bar{x}_g)^4}{100 \ln \sigma_g{}^4}$

Sorting (σ_g)		Skewness (Sk_g)		Kurtosis (K_g)	
Very well sorted	<1·27	Very fine skewed	<$^{-}$1·30	Very platykurtic	<1·70
Well sorted	1·27–1·41	Fine skewed	$^{-}$1·30 to $^{-}$0·43	Platykurtic	1·70–2·55
Moderately well sorted	1·41–1·62	Symmetrical	$^{-}$0·43 to $^{+}$0·43	Mesokurtic	2·55–3·70
Moderately sorted	1·62–2·00	Coarse skewed	$^{+}$0·43 to $^{+}$1·30	Leptokurtic	3·70–7·40
Poorly sorted	2·00–4·00	Very coarse skewed	>$^{+}$1·30	Very leptokurtic	>7·40
Very poorly sorted	4·00–16·00				
Extremely poorly sorted	>16·00				

Figure 6: From Blott and Pye (2001), showing formulas for calculating mean, standard deviation, skewness and kurtosis. Tables for interpretation.

All fractions were calculated using the sum of fractions within their size range (i.e. 10-63 µm for sortable silt fraction), according to the Udden-Wentworth classification of grain sizes based on the work of Udden (Udden, J.A., 1914) and Wentworth (Wentworth, C.K., 1922).

Sortable silt fraction (SSF) is an important parameter in sedimentology, since it has been shown to have a higher sensitivity to currents compared to clay which due to its cohesive nature requires more kinetic energy to erode, and coarser grains which are simply heavier (McCave et al., 2006). The >250 µm fraction corresponds to grain sizes with a diameter larger than fine sand (Wentworth, C.K., 1922). The %SSF in fine-grained range (0-63 µm), is a measure of how many percent of fine-grained sediments constitutes sortable silt. This was calculated by dividing the sortable silt fraction with the sum of fractions in the 0-63 µm range. This is useful in conjunction with mean SS size, which was calculated using the same method as mean grain size, but limited to 10-63 µm. During current-related winnowing, %SSF in fines decreases while mean SS size increases, and using both of them gives a strong indicator regarding current activity (McCave et al., 2006).

3 Results.

3.1 Obscuration test.

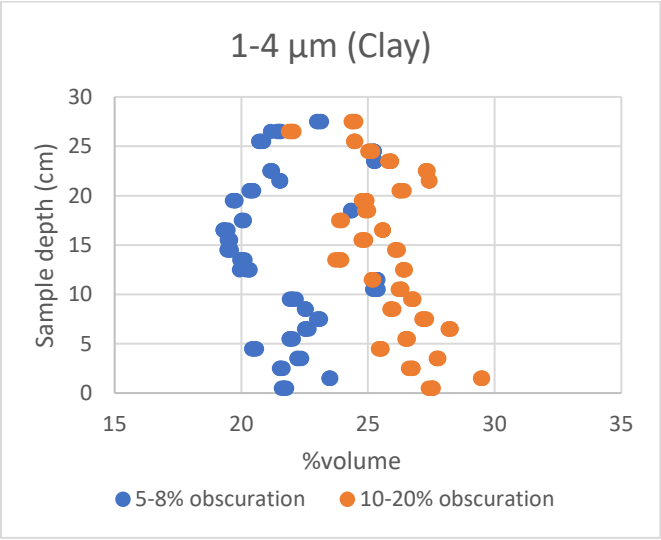

Figure 7: Clay fraction in SWERUS-L2-4-PC1 section 2, with higher vs lower obscuration. The higher obscuration method had minor increases in fraction, but with a similar trend. This increase could be due to multi-scattering.

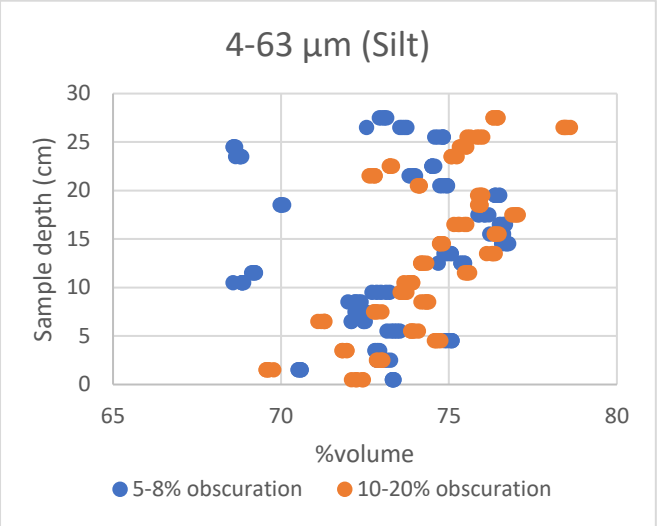

Figure 8: Silt fraction in SWERUS-L2-4-PC1 section 2, with higher vs lower obscuration. The lower obscuration method leads to more variable results.

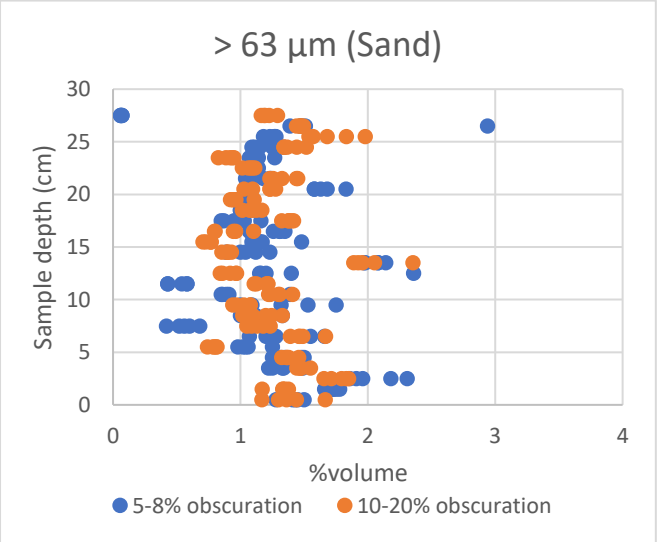

Figure 9: Sand fraction in SWERUS-L2-4-PC1 section 2, with higher vs lower obscuration. As with silt in Figure 8, the lower obscuration method yields a higher variation in fraction.

There was a small difference between lower and higher obscuration for the clay fraction (Figure 7) seen as a consistent increase of ~5 in %volume clay fraction, using the 10-20% laser obscuration method. Both methods yield the same pattern for the clay fraction. Silt (Figure 8) and sand fractions (Figure 9) show different patterns when comparing 5-8% with 10-20% obscuration, with the lower obscuration method having a higher degree of variability.

3.2 Grain size stratigraphy, SWERUS-L2-4-PC1.

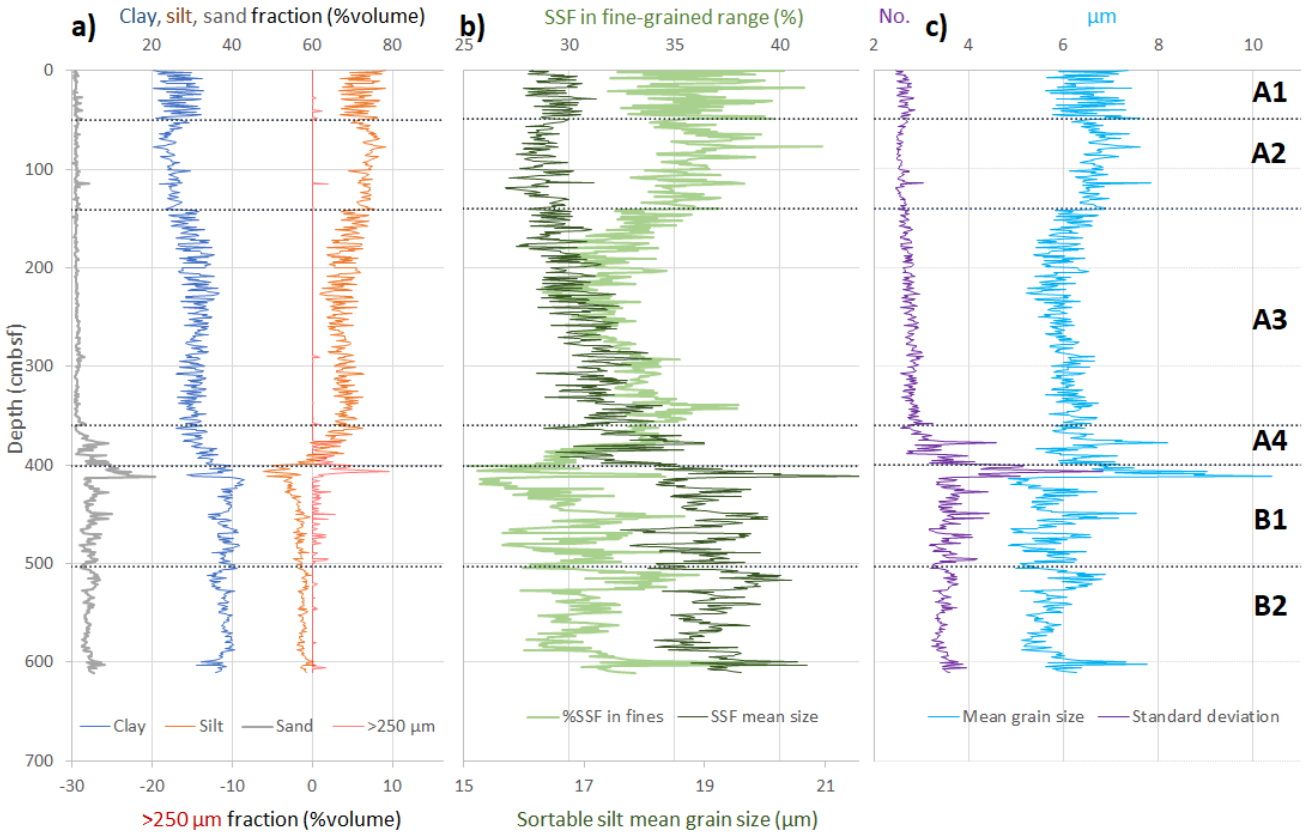

Figure 10: Grain size data plotted against depth. Lithological units are indicated on the right side. **a)** Grain size fractions. **b)** Sortable Silt Fraction, and the percentage of sortable silt in the fine-grained range. **c)** Mean grain size and standard deviation.

Jakobsson et al. (2017) identified two major lithologic units, A and B, in 4-PC1 based on magnetic susceptibility, bulk density and $\delta C^{13}_{org.}$ The grain size data is here used to identify four additional subunits of A. These are marked by broad zones containing differing trends in grain size fractions, sortable silt and mean grain size.

Down-core from 0 to 49.5 cm there is a relatively stable interval in the trend of %volume of size fractions, %SSF in fines, SSF mean, mean grain size and standard deviation. This is construed as subunit A1 (Figure 10). Subunit A2 is located between 49.5 and 140.5. Here, silt, SSF mean and %SSF in fines have a negative trend. There is a notable shift at 115.5 cm, where >250 µm reaches a fraction of 1.9% volume and is contemporaneous with a sharp increase in SSF mean, %SSF in fines, standard deviation and mean grain size.

Subunit A3, going down-core from 140.5 cm to 359.5 cm, is characterized by small shifts in fraction sizes, and increasing SSF mean through the whole subunit, while %SSF in fines decreases between 140.5 and ~240 cm before increasing again (Figure 10). The lower boundary of subunit 3 is taken as the tie line where more rapid changes in size fraction trends are observed (Figure 10). Subunit A4, spaced between 359.5 cm and 407 cm, has a notable increase in frequency and amplitude of sand and >250 µm fraction, along with rapidly decreasing silt down-core and an increase in clay. %SSF in fine-grained range show a strong down-core decline, while SSF mean size increases in the upper half and then decreases again (Figure 10). SSF mean size increases from ~18 to ~22 µm,

Below the transition from Unit A to B, at 407 cm, there is an abrupt shift where >250 µm fraction increases to 9.5 % volume, the highest in the record. Along with this, clay sees a positive shift of over 25% while silt decreases slightly (Figure 10). SSF mean size, %SSF in fines, mean grain size and standard deviation also exhibit an abrupt positive increase. A few centimetres down-core from this, at 412.5 cm, which is near the boundary between Units A and B, sand fraction more than quadruples along with an even greater increase in >250 µm fraction (Figure 10). Sand fraction decreases up-core from this, never again reaching similar levels. These shifts occur at the same depth as a sharp decline in clay fraction.

The division of subunits B1 and B2 was made by Jakobsson et al. (2017) and placed at 503-513 centimeters. This marked a major positive shift in magnetic susceptibility and bulk density down-core for B2 compared to B1. These units also constrain the different trends in the grain size data generated for this study, where subunit B1 is characterized by a higher frequency and amplitude changes in sand fraction. Subunit B2 exhibits less variation in sand fraction, albeit at an average amplitude similar to subunit B1, and more intermittent spikes in >250 µm fraction. Both SSF mean and %SSF in fine-grained range fluctuates more in regards to amplitude in Unit B. Mean grain size has a more negative trend down-core in subunit B2 as well, while the sorting is more stable for this subunit. While there are changes within B1 and B2, especially for sortable silt fraction mean and %SSF in fine-grained range, there are too many fluctuations to further subdivide this section of the core into more subunits in a useful fashion for the scope of this study.

3.2 Grain size stratigraphy, SWERUS-L2-5-GC1.

Figure 11: Grain size data plotted vs. Depth for SWERUS-L2-5-GC1 (including core-catcher). Segments without any lines are due to sediment being removed by previous investigators. Lithological units indicated by letters to the right. **a)** Grain size fractions. **b)** Sortable silt fraction and percent sortable silt fraction in fine-grained range. **c)** Mean grain size & Standard deviation, calculated using the Geometric Method of Moment (Blott and Pye, 2001).

While the units of 5-GC1 can be hard to correlate with 4-PC1, due to the difference in length, which may be due to compaction, erosional variations and different sedimentation rates, the positive shifts in sand and coarser fractions at ~92 cm (Figure 11) bears a strong resemblance to the one at ~407 cm in 4PC1 (Figure 10), also seen in increasing mean grain size and standard deviation. Therefore, the main units A and B from 4-PC1 have been employed here, but since the delimiter between units A and B in 4-PC1 were above the abrupt grain size variation, the correlation between 4-PC1 and 5-GC1 should be treated with care. No further subunits in B were used due to the difference in resolution making an assessment of subunits uncertain.

General differences and similarities can be observed in comparison between the two cores. Sand fraction is overall higher in 5-GC1 (Figure 11) than 4-PC1 (Figure 10), never reaching zero. It should be noted that the low laser obscuration method was used for 5-GC1, which can account for this difference. Mean grain size shows a pattern similar to the one in 4-PC1 (Figure 10), decreasing up-core through unit A, but showing a positive trend again in the upper 10-20 cm of the core (Figure 11).

4 Discussion.

4.1 Laser obscuration.

The MasterSizer3000 manual states that the danger of too high obscuration is multi-scattering, where the laser is diffracted at larger angles, which is interpreted by the MasterSizer3000 as fine-grained particles. The clay fraction (Figure 7) shows that the higher obscuration method had a small but consistent increase in fine-grained sediment, making it possible that multi-scattering occurs already at 10-20% laser obscuration. However, the grain size trends are similar with both 5-8% and 10-20% laser obscuration, which implies that even if there is multi-scattering, it does not adversely affect the ability to see changes in %volume of fractions.

4.2 Interpretation of grain size variations in Herald Canyon Cores.

There is evidence for onlap in reflectors 2, 3 and 4, as seen in their slope over the older, more steeply dipping acoustically chaotic strata below reflector R2 (Figure 4). This is a typical feature of transgressive systems tracts, as beach-erosion by waves deposit sediment off-shore. These are associated with lithological unit B. The oldest age in 4-PC1 based on the age model is at ~13,500 cal yr BP, while the oldest measured date is ~11,700 cal yr BP. This implies that the coring site was at a depth of more than 70 meters below sea level when the lowermost sediments in the core were deposited (Figure 3). At a depth of 70 mbsl, the flank of Herald Canyon bordering 4-PC1 would have been very close to sea level. Therefore, the onlap in the seismic data can be interpreted as due to shore-related transgression, with wave action progressively eroding the shoreline and depositing sediments off-shore beyond the slope break. Although the mean grain size is low, the sediments from Unit B have a higher coarse-grained fraction than those in Unit A. They also have a lower amount of %SSF, and a higher mean SS size (Figure 10). These observations are consistent with deposition in a current controlled higher energy environment.

Based on the strong positive increase in sand and coarser fractions in the lowest centimeters of 4-PC1 (Figure 10), they are a likely indicator that reflector R2 was penetrated, but it could also be an artifact from core recovery.

The age model indicates that between 400.5 and 399.5 cm, there is a temporal change in 4-PC1 from ~11,000 cal yr BP to ~3,600 cal yr BP just above reflector R5 (Figure 4). Since the age model is based on 8

age-depth datums in the core (Jakobsson et al., 2017), the nature of this transition, if it's due to a hiatus (erosional or non-depositional) or condensed sedimentation, can't be concluded from age estimations alone (Figure 5). The grain size data from 4-PC1 (Figure 10) show an abrupt change at ~407 cm, with a large positive shift in mean grain size, sand and >250 μm fraction, along with increasing sortable silt mean size. The positive SSF mean size gives an indication of current-related winnowing, even though a decrease in %SSF in fines would support this even further (McCave et al., 2006).

The age at 407 cm for 4-PC1 is estimated to ~11,000 cal yr BP (Figure 5), implying that the site was at ~70 mbsl (Figure 3) at that time. At this depth, erosion is unlikely to be an effect of shore-related transgression. Jakobsson et al. (2017) argued that the transition from Unit B to Unit A marked the submergence of Beringia Land Bridge and first inflow of Pacific water into the Arctic ocean during the Holocene. One possibility is that the erosional horizon occurred due to the opening of Bering Strait. The abrupt shift at ~407 cm in 4-PC1 might be related to an increase in paleocurrent velocity as Pacific water started to flow into Herald Canyon. Paleodepth models show that the only pathway for Pacific water to flow north of the Chukchi Sea, was located at Herald Canyon (Figure 12). It is likely that this kind of topographical channeling led to current velocities that developed from having a winnowing effect to erosion. Since water with higher salinity is denser, the Pacific inflow might have been directed along the ocean floors and down into Herald Canyon. The erosional feature therefore seems to be related to currents caused by the submergence of the Beringia Land Bridge, which in turn was due to deglaciation-related sea level increase.

The extrapolated age model for 4-PC1 suggests a return to sediment accumulation at ~3,500 cal yr BP (Figure 5). This coincides with sea levels and rates of rise similar to present ones (Figure 3). Up-core from the unit A/B boundary, there is a steady decrease in SSF mean size and increasing %SSF in fines, only stabilizing at subunit A2 which corresponds to the last 1,000 years (Figure 4). This is a strong indicator of decreased winnowing. The resumed sediment accumulation is therefore contemporaneous with decreasing current velocities, decreased transgression rates and a sea level within 5 m of current level (Figure 3).

Mean grain size from both 4-PC1 (Figure 10) and 5-GC1 (Figure 11) decreases up-core from the boundary between unit A and B, until subunit A2 which corresponds to ~1,000 cal yr BP, where it starts to increase again. This appears to be caused by decreased clay content and increase in the fine silt fraction (Figure 10). These grain size changes appear independent of sea level, which has not changed substantially during the past 1000 years (Figure 3). Therefore, it is unclear what may have caused increased fine sediment accumulation in the past 1000 years.

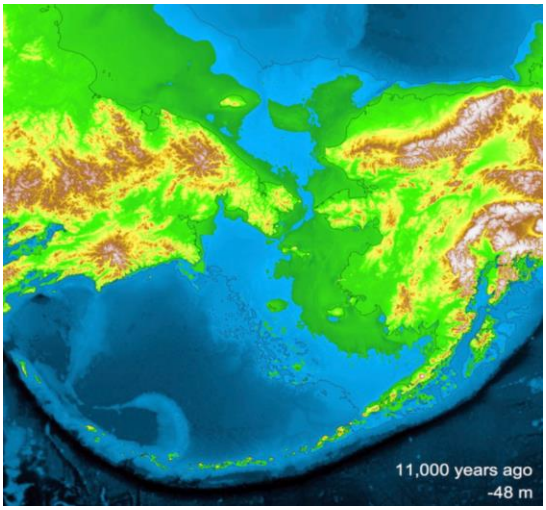

Figure 12: A model of paleodepths at 11,000 cal yr BP. From Manley, W.F., 2002.

5 Conclusions.

At ~407 cm in 4-PC1 from the Herald Canyon, Chukchi Sea, there is an abrupt change in sediment lithology signaling the start of a transition from near-shore to marine conditions. It is interpreted to mark the opening of the Bering Strait during marine transgression after the Last Glacial Maximum. Detailed grain size data indicates that the base of this transition was marked by a period of winnowing followed by erosion between ~11000 to ~3,500 cal yr BP. Considering the age of sediments below the erosional surface (>11,000 cal yr BP), the coring site was too deep to be influenced by wave base erosion. Therefore, erosion likely occurred in response to the opening of Bering Strait, which led to inflow of saline Pacific water that was initially channeled through the Herald Canyon. Grain size in sediments deposited after the resumed accumulation indicate weakening of currents after ~3,500 cal yr BP.

6 Acknowledgements.

Thanks goes to Matt O'Regan, Henrik Swärd and Christof Pearce for their supervision of the project, and to Carina Johansson for assisting with sediment core logistics to and from the lab and preparation of chemical compounds.

7 References.

Blott, S.J., and Pye, K., 2001. Gradistat: A Grain Size Distribution and Statistics Package for the Analysis of Unconsolidated Sediments. Earth Surf. Process. Landforms 26, 1237-1248. doi: 10.1002/esp.261.

Cronin, T.M., O'Regan, M., Pearce, C., Gemery, L., Toomey, M., Semilietov, I., and Jakobsson, M., 2017. Deglacial sea-level history of the East Siberian Sea Margin. Clim. Past Discuss. 1-21. doi: 10.5194/cp-2017-19.

Dyke, A. S. and Savelle, J. M.: Holocene History of the Bering Sea Bowhead Whale (Balaena mysticetus) in Its Beaufort Sea Summer Grounds off Southwestern Victoria Island, Western Canadian Arctic, Quaternary Research, 55, 371-379, 2001.

Elias. S.A., Short, S.K., and Phillips, R.L.: Paleoecology of late-glacial peats from the bering land bridge, Chukchi Sea shelf region, northwestern Alaska, Quaternary Research, 38, 371-378, 1992.

Jakobsson, M., Pearce, C., Cronin, T.M., Backman. J., Anderson, L.G., Barrientos, N., Björk, G., Coxall, H., de Boer, A., Mayer, L.A., Mörth, C.M., Nilsson, J., Rattray, J.E., Stranne, C., Semilietov, I., O'Regan, M., 2017. Post-glacial flooding of the Beringia Land Bridge dated to 11,000 cal yrs BP based on new geophysical and sediment records. Clim. Past Discuss. 1-22. doi: 10.5194/cp-2017-11.

Keigwin, L. D., Donnelly, J. P., Cook, M. S., Driscoll, N. W., and Brigham-Grette, J.: Rapid sea-level rise and Holocene climate in the Chukchi Sea, Geology, 34, 861-864, 2006.

Lambeck, K., Rouby, H., Purcell, A., Sun, Y., and Sambridge, M.: Sea level and global ice volumes from the Last Glacial Maximum to the Holocene, Proceedings of the National Academy of Sciences, 111, 15296-15303, 2014.

Manley, W.F., 2002, Postglacial Flooding of the Bering Land Bridge: A Geospatial Animation: INSTAAR, University of Colorado, v1, Manley, W.F., 2002, Postglacial Flooding of the Bering Land Bridge: A Geospatial Animation: INSTAAR, University of Colorado, v1, http://instaar.colorado.edu/QGISL/bering_land_bridge (accessed: 01.06.17).

McCave, N., and Hall, R., 2006. Size sorting in marine muds: Processes, pitfalls, and prospects for paleoflow-speed proxies. Geochemistry Geophysics Geosystems 7, 1-53. ISSN: 1525-2027.

M. F. A.: New evidence from the western Canadian Arctic Archipelago for the resubmergence of Bering Strait, Quaternary Research, 70, 60-67, 2008.

Peltier, W. R. and Fairbanks, R. G.: Global glacial ice volume and Last Glacial Maximum duration from an extended Barbados sea level record, Quaternary Science Reviews, 25, 3322-3337, 2006.

Pickart, R. S., Pratt, L. J., Torres, D. J., Whitledge, T. E., Proshutinsky, A. Y., Aagaard, K., Agnew, T. A., Moore, G. W. K., and Dail, H. J.: Evolution and dynamics of the flow through Herald Canyon in the western Chukchi Sea, Deep Sea Research Part II: Topical Studies in Oceanography, 57, 5-26, 2010.

Udden, J.A.: Mechanical composition of clastic sediments, Bulletin of the Geological Society of America, 25, 655-744, 194.

Watanabe, E. and Hasumi, H.: Pacific Water Transport in the Western Arctic Ocean Simulated by an Eddy-Resolving Coupled Sea Ice-Ocean Model, Journal of Physical Oceanography, 39, 2194-2211, 2009.

Wentworth, C.K.: A scale of grade and class terms for clastic sediments. Journal of Geology, 30, 377-392, 1922.

Woodgate, R.A., Stafford, K.M., and Prahl, F.G.: A Synthesis of Year-Round Interdisciplinary Mooring Measurements in the Bering Strait (1990-2014) and the RUSALCA Years (2004-2011), Oceanography, 28, 47-67, 2015.